

4D Grid-fitting of UV-optical spectra of massive stars.

I. Numerical technique and its associated uncertainties

Blagovest V. Petrov and Svetozar A. Zhekov*
 Institute of Astronomy and NAO, Bulgarian Academy of Sciences
 72 Tsarigradsko Chaussee Blvd., 1784 Sofia, Bulgaria

October 8, 2024

Abstract

The best way to check the validity of our theories (models) is by direct comparison with the experiment (observations). In this study, we focus on addressing the numerical inaccuracies intrinsic to the process of comparing theory and observations. To achieve this goal, we built 4D spectra grids for Wolf-Rayet stars (WC and WN spectral classes) and Blue Supergiants (BSGs) characterized by low metallicity similar to that of the Small Magellanic Cloud (SMC). Utilizing these 4D grids, we developed and validated a fitting approach facilitating direct fits to observed spectra. Through rigorous testing on designated ‘test’ models, we demonstrated that the numerical precision of derived essential stellar parameters, including effective temperature, mass-loss rate, luminosity, and wind velocity, is not exceeding 0.05 dex. Moreover, the mean absolute deviation of the numerically derived stellar parameters is consistently below this threshold for objects with both weak (SMC grid) and strong winds (WC and WN grids), even in the presence of Gaussian noise. Furthermore, we explored the influence of unaccounted factors, including variations in the metal abundances, wind acceleration laws, and clumping, on the precision of the derived parameters. We found that the first two factors have the strongest influence on the numerical accuracy of the derived stellar parameters. Variations in abundances predominantly influenced the mass-loss rate for weak-wind scenarios, while effective temperature and luminos-

ity remained robust. We found that the wind acceleration law influence the numerical uncertainty of the derived wind parameters mostly for models with weak winds. Interestingly, different degrees of clumping demonstrated good precision for spectra with strong winds, contrasting with a decrease in the precision for weak-wind cases. We found also that the accuracy of our approach depends on spectral range and the inclusion of ultraviolet spectral range improves the precision of derived parameters, especially for object with weak winds.

Keywords: Techniques : numerical — Wolf-Rayet stars — OB supergiant stars — Stellar winds

1 Introduction

The extreme temperature and luminosities of the massive stars provide a large amount of ionizing photons, leading to extreme non-local thermal equilibrium conditions (non-LTE) in their expanding atmospheres. Additionally, mass-loss rate and velocity structure of the wind contribute to altering the density profile of the massive star atmospheres. This makes the spectral analysis of massive stars complex problem, achievable only after development of sophisticated model atmosphere codes.

By utilizing stellar atmosphere modelling, it becomes feasible to derive essential physical properties of massive stars. These include fundamental parameters such as effective temperature (T_*), luminosity (L_*), mass-loss rate (\dot{M}), and terminal wind velocity (v_∞). These essential parameters play a crucial role as inputs in various models related to stellar structure and evolution, necessitating ac-

*Email addresses: bpetrov@astro.bas.bg (Blagovest Petrov); szhekov@astro.bas.bg (Svetozar Zhekov)

curate knowledge of their values.

Typically, the interpretation of spectra from massive stars strongly relies on model atmospheres and a precise spectroscopic analysis should incorporate multi-wavelength comparison between observations and models. Currently, there is no established standard approach for deriving stellar parameters using the complete spectra information and different studies often have significantly different results. In general, such discrepancies may be attributed to disparities in atomic data, model atmosphere codes, numerical methods and/or analysis techniques. Nonetheless, adopting a consistent approach that incorporates the full spectral information in parameter derivation has the potential to produce more comparable results and enhance our understanding of the evolution of massive stars.

Over the past decades, there has been significant progress in computer hardware and astronomical software. This allowed for the inclusion of iron line blanketing and microclumping in the models (Hillier & Lanz 2001; Gräfener et al. 2002) leading to producing more realistic stellar spectra. The realism of these spectra can be revealed solely through direct comparison of the theory with observed data. Given the complexity of the stellar atmosphere models, we must have a *tool* (e.g., *numerical technique*) to carry out such a comparison. Three primary sources of inaccuracy arise during this comparison: a) inaccuracies inherent in the theory; b) inaccuracies introduced by the experiment (observations); c) inaccuracies of the numerical technique for comparing theory and observations. For the latter, the terms numerical uncertainty, numerical precision and numerical accuracy will be used throughout the text. Evaluating the overall accuracy of the model lies beyond the scope of our research. In this study, our emphasis is placed on addressing the numerical inaccuracies resulting from the process of comparing theory and observations: item c) above. This task is fundamentally significant because it serves as a bridge connecting theory with observations. If our method of comparing theory and observations bears significant uncertainties, it could obscure the interpretation of the physical parameters we derive, regardless how accurate our theory and observations are.

To achieve this goal (evaluation of uncertainties of the numerical technique for comparing theory and observations), we need a ‘work field’. So, we have calculated

four-dimensional grids of stellar atmosphere models for massive stars, aiming to develop and access a rigorous method for deriving stellar parameters through the direct fitting of observed spectra. The four ‘axes’ of these grids are effective temperature (T_*), luminosity (L_*), mass-loss rate (\dot{M}), and terminal wind velocity (v_∞). Although it is well known, we recall that such a choice of basic parameters is due to the fact that the spectrum of a massive star is determined by the ionization structure of its wind. At a given point in the stellar wind, the latter basically depends on the ratio of the ionizing photons to the gas number density. The stellar luminosity and the stellar temperature (controlling the shape of the underlying continuum) are responsible for the available ionizing photons. The mass-loss rate and the wind velocity of the massive star are the factors that set the gas number density, as the latter determines the shape of the line profiles in the spectrum.

The spectral grid-modelling may adopt ‘lighter’ grids (e.g., 3D grids; three-dimensional), provided we have a priori information on some of the basic stellar parameters. It is our understanding that this is possible only for the terminal wind velocity of a massive star and in such a case all the model spectra in the 3D grid will have the same value of the stellar wind. However, such a 3D grid will have limited applications: it is suitable only for analysis of the specific object at hand or of spectra of massive stars with stellar wind velocities not very different from the value adopted in the corresponding 3D spectral grid. An illustrative application of a three-dimensional grid and its use for determining fundamental physical parameters is found in the study by Zhekov et al. (2020).

We note that ‘lighter’ spectral grids have been actively used in the last two-three decades or so, as the case of the Potsdam Wolf-Rayet Models¹ is probably the best example of using the stellar atmosphere models for deriving stellar parameters of an appreciable number of massive stars in a consistent manner (Hamann et al. 2019; Sander et al. 2019 and references therein). However, these are two-dimensional (2D) grids and their use relies on analysis of spectra, normalized to continuum. On the one hand, this makes the comparison between theory and observations more efficient in sense of technical (computer) resources. On the other hand, it adopts some ap-

¹<https://www.astro.physik.uni-potsdam.de/~wrh/PoWR/powrgrid1.php>

proximate relations (scaling laws) for the stellar parameters, that is it is done at the expense of not using all the available information about the physical conditions in the spectral-formation regions (stellar winds). Thus, our choice for a ‘work field’ in this study is to make use of 4D grids of spectral models of massive stars.

This paper is organised as follows: In Section 2, we describe the employed model of stellar atmospheres and outline the approach developed for directly fitting the stellar spectra. In Section 3, we evaluate the expected accuracy of the derived stellar parameters by fitting ‘test’ spectra of models with randomly chosen values of stellar parameters. In Section 4 we discuss the possible implication of our results. We present our conclusions in Section 5.

2 Spectral modelling

2.1 The model of stellar atmosphere

For the purposes of our investigation, we use the non-LTE radiative transfer code `CMFGEN` (Hillier & Miller 1998; Hillier & Lanz 2001).² This software is a comprehensive atmosphere code that incorporates full line-blanketing, specifically engineered to address the challenges posed by solving the statistical equilibrium and radiative transfer equations in spherical geometry.

In `CMFGEN`, the determination of a stellar effective temperature follows the Stefan-Boltzmann law with a reference radius specified at a particular value for the Rosseland optical depth. For OB stellar models, we have opted for a reference optical depth of 2/3, whereas for WN and WC stars, given their strong winds, we have chosen a reference optical depth of 20. This choice ensures that the stellar radii do not extend into the wind region. The formula for computing the effective temperature is as follows:

$$T_* = \left(\frac{L}{4\pi\sigma R_*^2} \right)^{1/4} \quad (1)$$

Here, L denotes the stellar luminosity, σ is the Stefan–Boltzmann constant, and R_* is the specified radius for the reference Rosseland opacity.

From observations, we know that the winds of massive stars exhibit non-uniform characteristics, characterized

by the presence of inhomogeneities or ‘clumps’. These clumps have a notable impact on the appearance of stellar spectra, making it imperative to model non-uniform stellar atmospheres.

`CMFGEN` provides a mechanism to account for optically thin clumping, often referred to as microclumping. This approach is grounded in the concept that the stellar wind is composed of clumps characterized by heightened density and dimensions smaller than the mean free path of photons. These clumps possess an increased density, expressed as a clumping factor denoted as D , in comparison to the average wind density. The models are calculated with the assumption that the clumps are created by a volume filling factor represented by the reciprocal of D , which is designated as f , assuming that the regions between clumps contain minimal matter. This factor is related to the volume filling factor, and it follows the relationship $f = 1/D$, assuming that the region between the clumps is essentially devoid of matter.

In our models, $f_\infty = 0.1$, described by the following clumping law:

$$f(r) = f_\infty + (1 - f_\infty)e^{-v(r)/v_{cl}} \quad (2)$$

Here, r is the distance from the star, $v(r)$ is the wind velocity and v_{cl} is its value from which clumping is taken into account. We have chosen the clumping to start at $v_{cl} = 30 \text{ km s}^{-1}$.

It is important to note that `CMFGEN` does not solve the wind momentum equation. Consequently, the structure of the wind velocity must be predefined. In our models, we describe the wind velocity structure using a standard β -type velocity law with a specific exponent, which is set to $\beta = 1$. This velocity law is connected to the hydrostatic section of the wind, situated just below the sonic point, where the wind velocity attains the local speed of sound. We note that the turbulent gas velocity (v_{turb}) contributes to the ‘micro-structure’ of the wind, and a specific value must be adopted.

Selecting uniform values for the volume filling factor, velocity-law exponent and turbulent velocity is done with the intention of reducing the number of independent parameters within the models. Adopting uniform parameter values of β , f_∞ and v_{turb} can be regarded as conventional in the field of spectral modelling for massive Wolf-Rayet stars (e.g., Hamann et al. 2019 Sander et al. 2019

²<https://sites.pitt.edu/~hillier/web/CMFGEN.htm>

and references therein). It is important to acknowledge that there may be valid reasons to explore alternative values for these parameters in specific situations. This approach could be justified when seeking a closer alignment with actual physical conditions and observational data.

2.2 Description of WN, WC and BSG grids

The spectral characteristics of a massive star are intricately tied to the ionization structure of its stellar wind. Broadly speaking, the ionization state within a specific region of the stellar wind depends on the equilibrium between the quantity of ionizing photons and the density of gas in that region. While, the primary sources of ionizing photons in the stellar wind are generally the stellar luminosity and temperature, density structure of the wind is predominantly determined by the mass-loss rate and wind velocity. Consequently, these four parameters (L_* , T_* , \dot{M} and v_∞) serve as the fundamental physical parameters defining the features of stellar spectra. Therefore, we have chosen these parameters as the primary inputs for our model grids.

Considering all of this and the needs of our future studies, we have calculated model grids for nitrogen-rich (WN) and carbon-rich (WC) Wolf-Rayet stars, as well as Blue Supergiants (BSGs) characterized by low metallicity similar to the Small Magellanic Cloud (SMC). Throughout the text, we will denote them WC grid, WN grid and SMC grid. Each `CMFGEN` model in our grids incorporate the of elements of H, He, C, N, O, Ne, Mg, Al, Si, P, S, Ar, Ca, and Fe.

The chosen parameter ranges for varying L_* , \dot{M} , v_∞ and T_* are well-suited for these objects and are as follows.

For the WN grid, we selected $\log \dot{M} = [-5.0, -4.8, -4.5, -4.3]$ \dot{M} in $M_\odot \text{ yr}^{-1}$, $\log L_* = [5.0, 5.2, 5.4, 5.6, 5.8, 6.0]$ L_* in L_\odot , $T_* = [40\,000, 45\,000, 50\,000, 55\,000, 60\,000, 65\,000]$ K and $v_\infty = [1\,000, 1\,500, 2\,250]$ km s^{-1} , resulting in a total number of 432 model spectra. The adopted WN abundances are from van der Hucht et al. (1986).

For the WC grid, we selected $\log \dot{M} = [-5.0, -4.8, -4.5, -4.3]$ in $M_\odot \text{ yr}^{-1}$, $\log L_* = [4.8, 5.2, 5.4, 5.6, 5.8]$ L_* in L_\odot , $T_* = [45\,000, 50\,000, 55\,000, 60\,000, 65\,000, 70\,000, 80\,000, 90\,000, 100\,000, 110\,000, 120\,000]$ K and $v_\infty = [1\,500, 2\,000, 3\,000]$ km s^{-1} , resulting in a total number of 792 model spectra. The adopted WC abundances are from van der Hucht et al. (1986).

For the SMC grid, we selected $\log \dot{M} = [-7.00, -6.75, -6.50, -6.25, -6.00]$ in $M_\odot \text{ yr}^{-1}$, $\log L_* = [5.00, 5.25, 5.50, 5.75]$ L_* in L_\odot , $T_* = [15\,000, 17\,500, 20\,000, 22\,500, 25\,000, 27\,500]$ K and $v_\infty = [500, 1\,000, 1\,500, 2\,000, 2\,500]$ km s^{-1} , resulting in a total number of 600 model spectra. The adopted He abundance is 25% by mass, while the other elements have metallicity of $[\text{Fe}/\text{H}] = -0.95$ dex (Choudhury et al. 2018). We are currently working to further extend this grid to Galactic metallicities.

For the turbulent velocity, a value of $v_{\text{turb}} = 20 \text{ km s}^{-1}$ throughout the wind is used for the Wolf-Rayet grids, while a value of $v_{\text{turb}} = 10 \text{ km s}^{-1}$ is used for the SMC grid.

2.3 4D grid modelling - a new approach to direct non-linear fitting of stellar spectra

The objective of this study is to develop a numerical methodology for grid-fitting stellar spectra of massive stars and estimate its corresponding numerical uncertainties. To accomplish this objective, it is crucial to compare theoretical and fitted spectra with established stellar parameters. However, in reality this is not possible, and associated uncertainties from numerical fitting techniques often remain ambiguous. It is only through a clear understanding of these associated numerical uncertainties that we can gauge the reliability of any parameters derived from the comparison of theoretical spectra with real observations.

As already demonstrated (Zhekov et al. 2020), our choice is to carry out *direct* fitting of an observed spectrum with a theoretical spectrum ‘extracted’ from a grid of theoretical spectra (Section 2.2). In that study, we used 3D spectral grids while we deal here with technically more complex (but physically more sophisticated) case of 4D grids. Thus, our fitting procedure has two parts: (a) how we calculate a model spectrum, using a 4D spectral grid; (b) how we estimate the ‘similarity (correspondence)’ between the observed and theoretical spectra. It is important to emphasise that for fitting procedures of this nature, whether working with absolutely calibrated observed spectra or observed magnitudes (i.e. using spectral energy distribution), a crucial requirement is having knowledge of the distance to the studied object.

It's important to mention that our fitting procedure operates in log-log space. In other words, each applied interpolation works with the logarithm of the dependent function (specifically, the spectrum, which represents the spectral density) and the logarithm of the independent variable. By such a choice, all the approximations result in physically meaningful (i.e., positive) values for the function (i.e., spectral density).

Calculating a model spectrum. In our model grids, we provide *precise* spectra exclusively at the grid nodes. Nevertheless, to generate spectra for parameter values that fall between these nodes, we must utilize an approximation method.

We tried various approximations and found that the most reliable, that is the most stable and with acceptable accuracy, is linear interpolation in the log-log space. Since we deal with 4D grids, by analogy with the 2D case, for which the standard procedure could be the bi-linear interpolation we perform *quatro*-linear interpolation. So, if we want to calculate a spectrum for a set of stellar parameters $(T_*, \log \dot{M}, \log L, v_\infty)$ that fell in a specific 4D 'cube', we perform linear interpolation consecutively from 1D through 2D and 3D up to 4D, that is along all the 'axes' of the 4D 'cube' (Fig. 1 presents a schematic diagram of the *quatro*-linear interpolation). We recall that the bi-linear interpolation is of higher order (higher accuracy) than the linear approximation (e.g., see sec. 3.6 in Press et al. 1992), thus, the adopted *quatro*-linear interpolation is of higher order (higher accuracy) than the bi-linear interpolation. An important detail is the choice of the independent variable for the interpolation process.

Understandably, the basic case is to choose the logarithm of actual physical parameters as independent variables for the *quatro*-linear interpolation (linear interpolation along each dimension of the 4D grid). Let us denote it 'basic approximation' or B-approximation.

On the other hand, since the line emission is a very important feature in the spectra of massive stars of early types, we consider two other cases of the independent variable: the emission measure scale and the transformed radius. Those two are somehow indicative of the stellar wind emission. We denote these cases EM-approximation and RT-approximation, respectively.

We note that the emission processes that take place in formation of the stellar wind emission are two-particle collisions. So, it is natural to expect that line and contin-

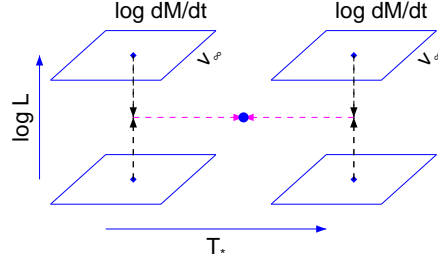


Figure 1: Schematic diagram of the *quatro*-linear interpolation. To calculate a model spectrum defined by a set of stellar parameters $(\log \dot{M}, v_\infty, \log L, T_*)_0$, marked by a filled-in circle in blue colour, we make the following steps. First, we run linear interpolation along the $\log \dot{M}$ and v_∞ axes to calculate the spectra at the $(\log \dot{M}, v_\infty)_0$ point in the four squares in blue colour. Then, we perform two linear interpolations along the $\log L$ axis to get the spectra at the $\log L_0$ points (marked by dashed lines and arrows in black). Finally, we derive the spectrum at the point of interest by a linear interpolation along the T_* axis (marked by dashed lines and arrows in magenta colour).

uum emission of various ionic species to be proportional to the emission measure scale:

$$EM_S = n^2 V = \left(\frac{\dot{M}}{v_\infty}\right)^2 R_*^3 = \left(\frac{\dot{M}}{v_\infty}\right)^2 \frac{L^{3/2}}{T_*^6} \quad (3)$$

where n is the gas number density and V is the corresponding volume for a specific ion, and each line-emission volume is proportional to the third power of the reference radius (R_* , see eq. 1), because the latter sets the scale of the emission region in the stellar wind of a massive star.

The term transformed radius (R_r) was introduced by Schmutz et al. (1989) and has been used in modelling of observed spectra of massive stars (see Hamann et al. 2019, Sander et al. 2019 and references therein). And, in

terms of stellar parameters it reads:

$$R_t = R_* \left(\frac{v_\infty}{\dot{M}} \right)^{\frac{2}{3}} = \frac{L^{1/2}}{T_*^2} \left(\frac{v_\infty}{\dot{M}} \right)^{\frac{2}{3}} \quad (4)$$

where again we made use of eq. 1.

As seen from eqs. 3 and 4, both interpolation variables depend on all the basic stellar parameters considered in this study. Therefore, when performing grid interpolation, we can use any of these variables only for one of the ‘axes’ of our 4D grid that is directly responsible for the stellar wind emission (i.e., $\log \dot{M}$ and v_∞). So, for the EM-approximation and RT-approximation we use the corresponding interpolation variable on one of these two axes and we adopt linear interpolation for the rest three axes (as in the B-approximation).

As result, our fitting procedure has FIVE approximation cases to calculate a model spectrum based on a 4D grid of stellar atmosphere model spectra: one B-approximation, two EM-approximations and two RT-approximations.

Similarity between observed and theoretical spectra. A standard way in spectral fitting is to adopt some likelihood estimator (LE) in order to check how well a theoretical spectrum matches an observed one. As a rule, the minimum value of this likelihood estimator defines a set of fitting parameters reproducing the observed spectrum ‘best’. We explored spectral fitting with different likelihood estimators (χ^2 -minimization among others) and we achieved best results with estimators based on absolute deviations between the observed and theoretical spectra: $z_i = S p_{obs}(\lambda_i) - S p_{mod}(\lambda_i)$. Since we fit an observed spectrum, the model spectrum is subject to the interstellar extinction (reddening), that is we fit for five parameters: four stellar parameters T_* , $\log \dot{M}$, $\log L$, v_∞ and E(B-V).

Our fitting procedure adopts the following robust likelihood estimators:

$$\begin{aligned} LE_1 &= \sum_i |z_i| & LE_2 &= \sum_i \ln(1 + |z_i|) \\ LE_3 &= \sum_i \frac{|z_i|}{1 + |z_i|} & LE_4 &= \sum_i \tanh(|z_i|) \end{aligned} \quad (5)$$

LE_1 is the sum of the absolute deviations between the observed and model spectra, LE_2 is defined by analogy with the Cauchy distribution (e.g., see sec. 15.7 in

Press et al. 1992), LE_3 and LE_4 are experimental estimators that have the property to decrease the weight of the deviant points in the fit while searching for the minimum of a LE -function. We note that the LE_2 -, LE_3 - and LE_4 -function behaviour is similar to that of the standard LE_1 -function for small values of z_i , but LE_2 -, LE_3 - and LE_4 -functions are more robust for the deviant points. Such points might be a result both from the observational uncertainties as well as from uncertainties in numerical approximations.

On the technical side, we adopted the downhill simplex method to search for the minimum of the LE -functions as its algorithm is exemplified in the *amoeba* procedure (see sec. 10.4 in Press et al. 1992)³.

In summary, our 4D-grid fitting process consists of the following steps. First, an individual fit obtains the ‘best’ set of model parameters by making use of the five approximations previously described: one B-approximation, two EM-approximations and two TR-approximations. Namely, it picks up the result from that approximation which provides the smallest minimum of the LE -function at hand. Second, we carry out spectral fit for each of the four LE -functions defined above (see eq. 5). As a result, we derive four ‘best’ sets of stellar parameters that define a model spectrum matching the observed one. And, the mean of these four ‘best’ sets constitutes the solution from our fitting process.

3 Test results

The accuracy of the derived stellar parameters from 4D-grid fitting of observed spectra relies on the quality of the observed spectra and used fitting approach. An illustration of how 4D-grid fitting can be used to estimate stellar parameters from fitting an observed spectrum is provided in Appendix A. However, before estimating a reliable range of derived stellar parameters, it is imperative to investigate and establish the level of uncertainties arising from applying the fitting procedure.

³For each spectral approximation, we performed tests to compare results from *amoeba* procedure and those from a gradient method for searching the minimum of a function (e.g., Davidson-Fletcher-Powell algorithm, see sec. 10.7 in Press et al. 1992) and the derived ‘best’ sets of parameters were identical. So, we adopted the downhill simplex method in this study, because it does not require calculations of derivatives, thus, it introduces less numerical noise (uncertainties).

In order to investigate this, we carried out tests for each of the 4D grids of model spectra (WC, WN and SMC grid). Specifically, for each grid we calculated over 20 synthetic spectra using the `CMFGEN` code. These were used as ‘perfect’ observed spectra in the UV-optical domain. For each ‘perfect’ observed spectrum, we used a set of stellar parameters that were randomly chosen within the boundaries of the corresponding 4D grid. Each ‘perfect’ observed spectrum was subject to interstellar reddening, the value of which was randomly chosen as well. And, some fiducial value for the distance (e.g., 2000 pc) was associated with each object. We then fitted these test spectra to derive the corresponding stellar parameters. Differences between the *input* and *derived* values of the stellar parameters provide estimates of the expected accuracy from using our fitting procedure. Also, we performed additional tests by adding Gaussian noise to the ‘perfect’ observed spectra (‘noisy’ observed spectra), which could be considered more realistic representation of the observed spectra.

We note that stars with more strong winds (WN and WC grids) have in general UV-optical spectra that are richer in line emission than those with less weaker winds (SMC grid). So, we would expect that the stellar wind parameters for objects with strong winds would be derived with a better accuracy by our 4D-grid fitting procedure.

Objects with strong winds. Results from the tests for the ‘perfect’ observed spectra of WC and WN stars are shown in Figs. 2 and 3, respectively. Detailed results from these tests, along with those for the ‘noisy’ observed spectra, are presented in Table 1. It is evident that all the *absolute* deviations of the derived stellar parameters from their respected *input* values are well within the limits of (smaller than) 0.05 dex. Moreover, the mean absolute deviation for the WC and WN samples is significantly below 0.05 dex. However, we opt for a more conservative approach by assuming that the numerical uncertainty is determined by the maximum deviation observed in the tests (shown in the ‘max’ column of Table 1). Interestingly, this uncertainty limit (0.05 dex) also holds for the case of ‘noisy’ test spectra (Table 1).

Objects with weak winds. Figure 4 (‘perfect’ observed spectra) and Table 1 (‘perfect’ and ‘noisy’ observed spectra) present results from the tests for the SMC objects. As in the case of objects with strong winds, the mean absolute deviation of the derived stellar parameters is appreciably

less than the accuracy limit of 0.05 dex. However, we see that occasionally larger deviations occur (in $\sim 1\%$ of the cases).

In general, we may conclude that in both cases (strong and weak winds) numerical uncertainty of the derived stellar parameters is *not worse* than 0.05 dex. But, it is interesting to check whether the spectral range of the observed spectra may have some effect on the parameter accuracy as well.

Spectral range. Results from the tests for the ‘perfect’ observed spectra of WC, WN and SMC objects in the optical (3150 - 11000 Å) are given in Table 2. We see again that the numerical accuracy of the derived parameters is *not worse* than 0.05 dex for the objects with strong winds (WC and WN spectra). However, the quality of the derived parameters slightly deteriorates for the objects with weak winds (SMC spectra): the fraction of cases with parameter accuracy greater than 0.05 dex increases from $\sim 1\%$ to $\sim 8\%$.

Thus, it is reasonable to conclude that the larger the spectral range and the better the quality of the observed spectra of massive stars is, the better constrained are the derived stellar parameters from the 4D-grid fitting.

4 Discussion

It is essential to acknowledge that our fitting technique works within the framework of stellar atmosphere models, relying on certain assumptions about key properties such as chemical composition, wind velocity profile (β -law)⁴, and volume filling factor (clumping). What if the actual stellar properties do not correspond to those adopted in this study? It is indeed reasonable to expect some variation within a specific spectral class. Factors such as abundances, wind acceleration law, and clumping might display a degree of variability around presumed ‘typical’ values, falling within specified ‘typical’ limits.

Thus, we will next try to address in some detail this issue. We aim to explore the effect of conducting a 4D-grid fitting on observed spectra of objects whose abundances,

⁴In general, stellar rotation may influence the velocity profile of the wind and its structure (e.g., corotation interaction regions could also form), which will have an impact on the emergent spectrum. However, considering this case will require much more complex modelling: i.e., at least 2D stellar atmosphere models.

Table 1: Test results (absolute difference, Model - Fit), spectral range 1150 - 11000 Å.

Parameter	WC		WN		SMC	
	mean (dex)	max (dex)	mean (dex)	max (dex)	mean (dex)	max (dex)
‘Perfect’ spectra						
T_*	0.006	0.021	0.003	0.010	0.001	0.002
$\log \dot{M}$	0.008	0.019	0.006	0.020	0.016	0.047
$\log L$	0.006	0.029	0.004	0.012	0.002	0.007
v_∞	0.006	0.019	0.006	0.017	0.012	0.052
SNR \approx 100						
T_*	0.006	0.021	0.004	0.012	0.001	0.002
$\log \dot{M}$	0.008	0.019	0.007	0.020	0.014	0.058
$\log L$	0.006	0.029	0.005	0.013	0.002	0.005
v_∞	0.006	0.019	0.008	0.019	0.009	0.048
SNR \approx 50						
T_*	0.006	0.021	0.004	0.013	0.001	0.002
$\log \dot{M}$	0.008	0.019	0.006	0.020	0.014	0.055
$\log L$	0.006	0.029	0.005	0.013	0.002	0.006
v_∞	0.006	0.019	0.008	0.019	0.009	0.042
SNR \approx 25						
T_*	0.007	0.034	0.005	0.013	0.001	0.002
$\log \dot{M}$	0.008	0.020	0.007	0.020	0.016	0.077
$\log L$	0.007	0.028	0.006	0.014	0.003	0.007
v_∞	0.006	0.020	0.009	0.020	0.010	0.038

Notes. The labels WC, WN and SMC denote the tests for the WC grid, WN grid and SMC grid, correspondingly. The ‘mean’ and ‘max’ columns give the mean and maximum absolute difference between the input model parameter and its value derived from the fits. The SNR label denotes the mean signal-to-noise ratio of the model spectra with added Gaussian noise. The values given in bold are those that are beyond the boundary accuracy (0.05 dex) for the derived parameter. In each of those cases, there is only *one* value that is beyond the mentioned boundary, i.e. in $\sim 1\%$ of the SMC cases.

Table 2: Test results (absolute difference, Model - Fit), spectral range 3150 - 11000 Å.

Parameter	WC		WN		SMC	
	mean (dex)	max (dex)	mean (dex)	max (dex)	mean (dex)	max (dex)
	‘Perfect’ spectra					
T_*	0.006	0.021	0.003	0.012	0.001	0.002
$\log \dot{M}$	0.007	0.019	0.006	0.016	0.033	0.126
$\log L$	0.006	0.026	0.004	0.020	0.003	0.006
v_∞	0.006	0.017	0.006	0.017	0.035	0.192

Notes. All the columns and labels are as in Table 1. The values given in bold are those that are beyond the boundary accuracy (0.05 dex) for the derived parameter. There are 9 (nine) values in total that are beyond the mentioned boundary (5 for $\log \dot{M}$ and 4 for v_∞), i.e. in $\sim 8\%$ of the SMC cases.

wind acceleration laws, and clumping deviate from the values of these parameters adopted in our 4D grids.

4.1 Abundances

For each of the 4D grids considered in our study (WC, WN and SMC), we defined an additional abundance set labeled ‘Add.’ (Table 3).

The additional WC set is based on the WC abundances for galactic metallicity as defined in Sander et al. (2012) and the additional WN set represents the WN abundance set for galactic metallicity as defined in Hamann & Gräfener (2004) with helium mass fraction of 0.78.⁵ The additional SMC abundance set exhibits metal abundances that have approximately doubled (see Table 3 for details).

For each 4D grid, we prepared ‘perfect’ observed spectra having the same stellar parameters as described in Section 3, but their abundances were those from the ‘Add.’ set for WC, WN and SMC objects. We used our 4D-grid fitting procedure and the corresponding results are shown in Figs. 6, 7 and 8.

In general, changes in abundances affects the derived parameters and the most important change is in the derived values of the mass-loss rate. In the case of strong winds, i.e in the WN and WC grids, alterations in

$\log \dot{M}$ also result in corresponding changes in $\log L$. This is understood as the density profile, specific to a given chemical element in the stellar wind, undergoes changes solely due to variations in the mass-loss rate, the ionization structure must adapt in order to align with the observed spectrum. Consequently, the ionization agent (luminosity) is affected. In the case of weak winds, i.e SMC grid, there are practically no changes in the derived values of the effective temperature and luminosity (T_* and $\log L$). This is so since the stellar wind emission is not the dominant part of the spectrum, therefore, its changes does not lead to changes in the other stellar parameters.

4.2 Wind acceleration law

We recall that the 4D grids in this study were built adopting wind acceleration law, with $\beta = 1$. So for each 4D grid, we prepared two additional sets of ‘perfect’ observed spectra having the same stellar parameters as described in Section 3 and values of $\beta = 0.5$ and $\beta = 2$. This means that we explore the impact on the derived parameters if a massive star has a faster accelerating ($\beta = 0.5$) or a slower accelerating ($\beta = 2$) wind compared to that adopted in our 4D grids ($\beta = 1$).

The results from fits of these spectra with our 4D-grid fitting procedure are shown in Figs. 9, 10 and 11. It is evident that there are appreciable *systematic* changes in the derived stellar parameters. In general, their accuracy worsens. For strong winds, it could be assumed *not worse*

⁵See WC MW abundances and MW WNL-H20 abundances provided in the website of the Potsdam Wolf-Rayet models, <https://www.astro.physik.uni-potsdam.de/~wrh/PoWR/powrgrid1.php>

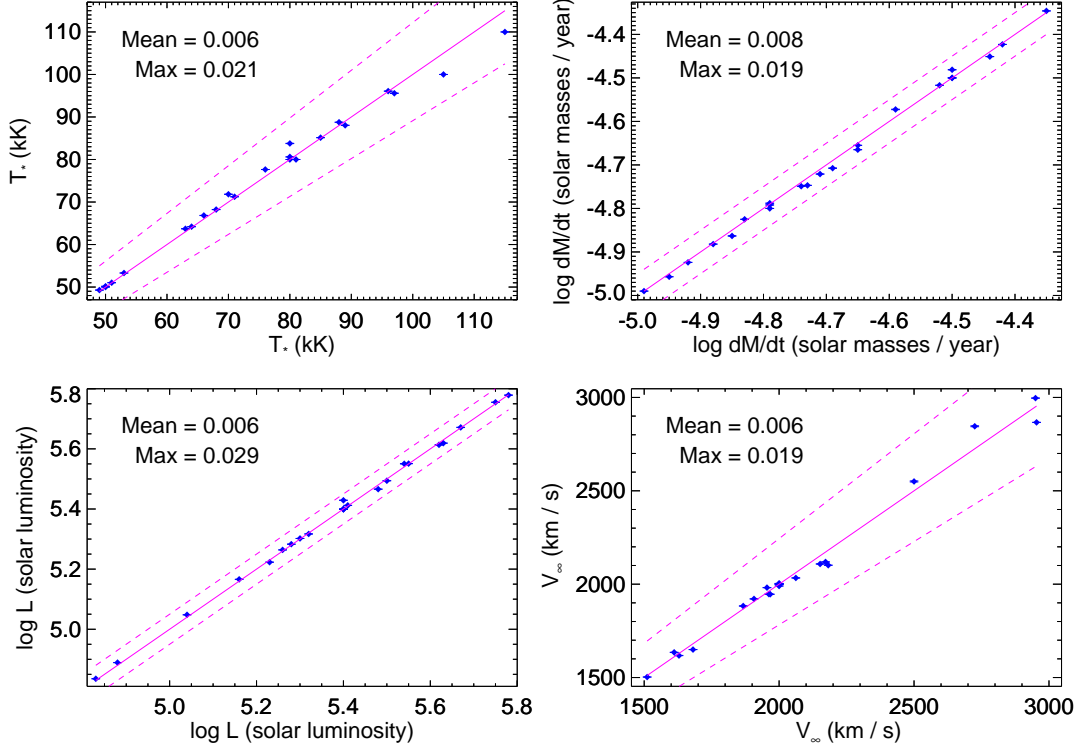


Figure 2: Test results for the WC grid (‘perfect’ observed spectra): effective temperature, mass-loss rate, luminosity and terminal wind velocity. Lines in magenta colour: (a) the solid line represents the perfect correspondence between the input model parameters and their values derived from the grid-modelling; (b) the two dashed lines represent the boundary for the ± 0.05 dex absolute deviation from the expected perfect correspondence. Mean and Max labels denote the mean absolute deviation for the test sample and its maximum value. Error bars are the standard deviation of the four minimizations adopted.

than 0.1 dex for all the stellar parameters. However for weak winds, the stellar wind parameters may have larger deviations (up to 0.2 dex) while the effective temperature and luminosity are recovered very well.

We think that the reason for such *systematic* changes is due to the fact that different β -laws result in considerable change of the velocity and density profiles of the stellar-wind plasma. Therefore, there are large changes in the ionization structure of the emission region of various ionic species as well. And, the 4D-fitting procedure tries to handle this within the available 4D grid. For example, if the ionization structure ‘moved in’ closer to the star, it chooses smaller stellar wind velocities and the oppo-

site is valid if the ionic structure ‘moved out’ further from the star. Next, it adjusts the amount of line emission by choosing the value of the mass-loss rate. In turn, different values of the latter may cause some changes in the derived values for luminosity. And, the effective temperature is no stranger here since its value also has some saying when it comes to ionization structure: it defines the ‘typical’ energy of the ionizing photons. In other words, the complex behaviour of the derived stellar parameters follows from the strong *non-linearity* of the physics involved in formation of the emission from massive stars of early spectral types.

Considering the significant impact of wind acceleration

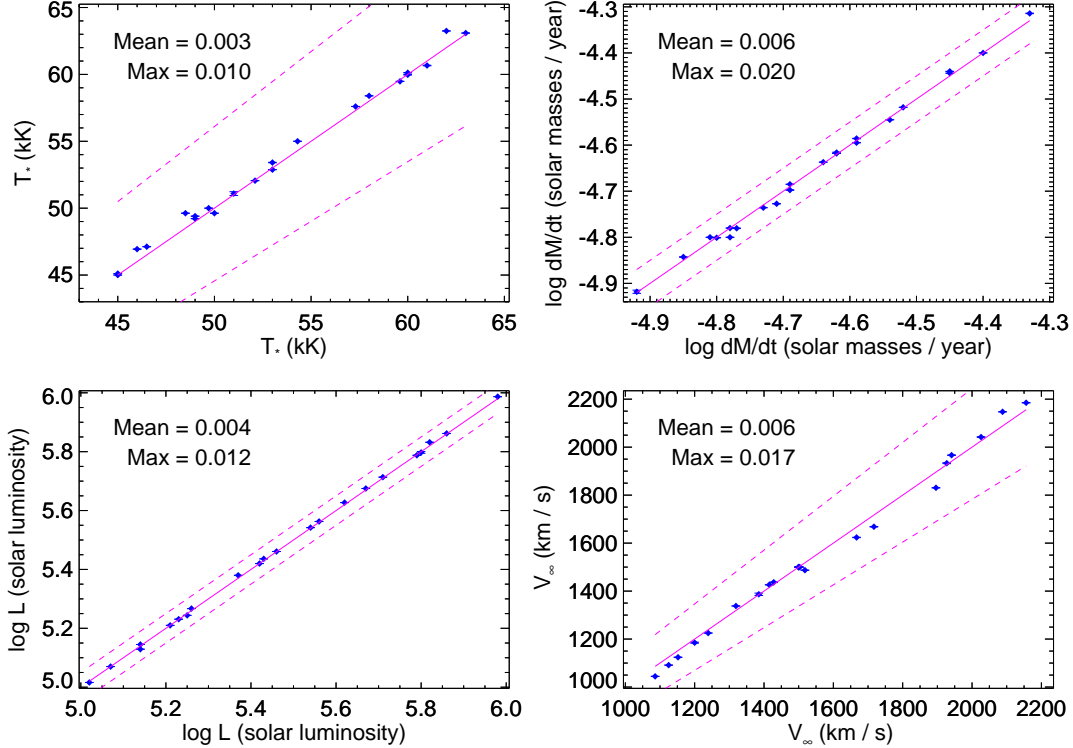


Figure 3: The same as Fig. 2 but for the WN grid (‘perfect’ observed spectra).

on the determined stellar parameters, we believe that the β -law could serve as a promising candidate for future expanding the grid-fitting procedure by adding another ‘dimension’.

It is worth recalling that the β -law is an approximation to the velocity profile in the winds of massive stars. A more realistic velocity profile can be modelled only if radiative hydrodynamics models are adopted. However, given their complexity and need of computer resources⁶, using such models to confront theory and observations by direct fitting of observed spectra of numerous specific objects does not seem feasible. Thus, we feel confident that

⁶When coupling radiative transfer and hydrodynamics, even the FASTWIND code (widely used to model the spectra of massive OB stars) is already not that fast according to its authors. The method is described in Sundqvist et al. (2019) and general description is found in the FASTWIND website <https://fys.kuleuven.be/ster/research-projects/equation-folder/codes-folder/fastwind>.

expanding our fitting procedure by adding the β -law ‘dimension’ is a reasonable step to take.

4.3 Clumping

It is generally assumed that massive stars with different mass-loss rates that scale with their corresponding volume filling factors ($\dot{M}_1/\sqrt{f_{\infty,1}} = \dot{M}_2/\sqrt{f_{\infty,2}}$) have very similar spectra, provided other stellar parameters are kept fixed. Our 4D fitting procedure relies on approximations of the model spectrum, leading to the introduction of numerical noise. To check the effect of the latter on this scaling law, we prepared an additional set of ‘perfect’ observed spectra having the same stellar parameters as described in Section 3 and a value of $f_{\infty} = 0.25$, however the mass-loss rates were scaled in accord with the scaling law: $\dot{M}_{new}/\sqrt{0.25} = \dot{M}_{old}/\sqrt{0.1}$ or $\log \dot{M}_{new} = \log \dot{M}_{old} + 0.2$. This means that the stellar parameters derived from apply-

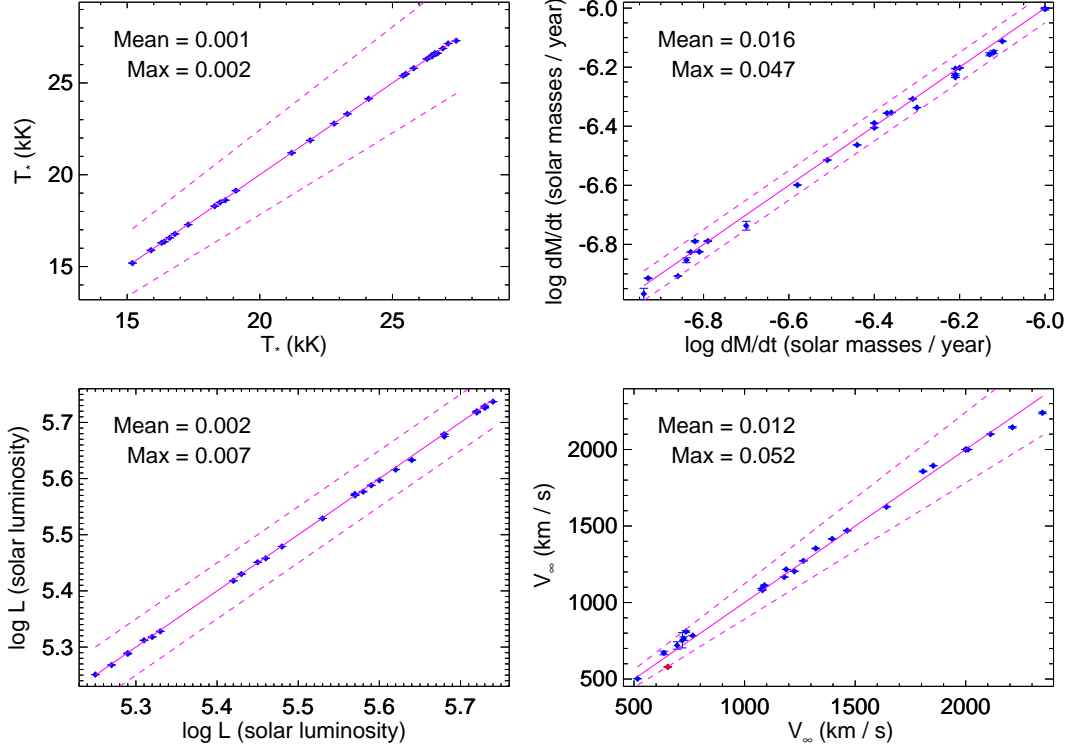


Figure 4: The same as Fig. 2 but for the SMC grid (‘perfect’ observed spectra). The derived parameters that have absolute deviation > 0.05 dex are given in red colour.

ing our 4D-grid fitting procedure should remain the same as before. The results from fits of these spectra are shown in Figs. 12, 13 and 14.

We see that for strong winds although there are some small *systematic* changes in the derived parameters, the clumping scaling law seems to be acceptably working: the derived stellar parameters are still within the numerical accuracy of 0.05 dex as before ($f_\infty = 0.1$). In contrast, when it comes to weak winds, the alteration in the mass-loss rate values is not insignificantly small. We attribute this behaviour to the imperfect nature of the clumping scaling law, where minor residuals are compounded with uncertainties arising from the numerical approximations to the model spectra adopted in our 4D-grid fitting procedure.

Note that stellar atmosphere models of massive stars typically assume a constant filling factor. However, a

physically more realistic approach would involve clumping that varies with distance from the star. Considering such variability becomes feasible when analyzing individual objects across diverse spectral domains like UV, optical and radio. An illustration of such approach can be found in Zhekov et al. (2020) (see also appendix A in that source).

Another fundamental assumption in these stellar atmosphere models is that the interclump medium has negligible contribution to the stellar spectrum, in other words, the intercloud space is ‘void of matter’ However, it seems improbable that such ‘empty’ space exists in the winds of massive stars. It is more likely that the winds of massive stars consist of a *two-component* flow: a massive component composed of clumps and a low-density component that fills the interclump space. Evidence supporting this two-component picture also arises from the analysis of X-

Table 3: Mass fraction of the most abundant chemical elements adopted in the spectral grids

Element	WC		WN		SMC	
	Main	Add.	Main	Add.	Main	Add.
X_H	3.84E-4	1.99E-3	1.60E-2	2.01E-1	7.48E-1	7.47E-1
X_{He}	3.22E-1	5.50E-1	9.53E-1	7.80E-1	2.50E-1	2.50E-1
X_C	3.88E-1	3.86E-1	3.66E-4	1.00E-4	2.67E-4	4.74E-4
X_N	1.83E-5	1.83E-5	2.10E-2	1.50E-2	7.86E-5	1.39E-4
X_O	2.50E-1	5.00E-2	1.12E-3	1.00E-5	6.51E-4	1.15E-3
X_{Ne}	3.02E-2	3.02E-3	3.16E-3	1.00E-5	1.43E-4	2.52E-4
X_{Fe}	1.72E-3	1.60E-3	1.70E-3	1.40E-3	1.47E-4	2.59E-4

Notes. The labels WC, WN and SMC denote the basic cases in this study. The ‘Main’ column gives the basic set of abundances used in the corresponding 4D grids and test models, while the ‘Add.’ column gives the abundances in the additional test models (see Sections 2.2 and 4.1).

ray emission from colliding-wind binaries, which are binary systems consisting of two massive stars (see discussion in section 4.3 of Zhekov et al. (2020)). We thus believe that addressing the possible emission from the low-density wind component (interclump matter) is needed and we plan to try carrying out even simple estimates in a future study.

5 Conclusions

We have calculated 4D grids of model spectra for early spectral class massive stars, specifically Wolf-Rayet stars (WC and WN spectral classes) and Blue Supergiants (BSGs) characterized with low metallicity similar to the one of Small Magellanic Cloud (SMC). These model grids served as the foundation for the development and testing of a fitting approach that enables *direct* fits to observed spectra. Through this approach, we demonstrated that essential stellar parameters such as effective temperature, mass-loss rate, luminosity, and terminal wind velocity can be derived with numerical precision not exceeding 0.05 dex. This was demonstrated with rigorous testing on designated ‘test’ models. Even when we added Gaussian noise to the synthetic spectra, the mean absolute deviation consistently remains notably below 0.05 dex for objects exhibiting both weak and strong stellar winds. This result is encouraging and provides robust support for our goal to derive basic stellar parameters from spectral analysis with

the highest attainable accuracy.

It is essential to note that the accuracy of the derived parameters depends on the spectral range and the inclusion of ultraviolet (UV) spectral range contributes to improved parameter derivations, particularly for objects with weak winds. This underscores the importance of selecting the spectral range for comprehensive and accurate stellar parameter determination.

We explored the influence of unaccounted factors, such as variations in metal abundances, the chosen wind acceleration law, and the degree of clumping, on the precision of the derived parameters. Notably, we found that variations in abundances predominantly affected the derived values of the mass-loss rate, particularly evident in scenarios with weak winds represented by our SMC grid. Interestingly, for weak winds, the derived values of effective temperature and luminosity remained largely unaffected by changes in abundances.

Furthermore, our tests revealed the significant influence of wind acceleration law on the accuracy of determined stellar parameters, with a noticeable decrease in precision, particularly up to 0.2 dex for objects with weak winds. In contrast, the application of different degree of clumping demonstrated good parameter precision (less than 0.05 dex) for objects with strong winds, but resulted in decreased precision up to 0.2 dex for objects with weak winds. This dichotomy underscores the interplay between the degree of clumping and the strength of stellar wind,

emphasizing the need for careful consideration of these factors in the pursuit of precise stellar parameter determinations. Consequently, our results affirm that the clumping scaling law is effective for objects characterized by strong winds, whereas its application to objects with weak winds results in a significant decline in precision, up to 0.2 dex.

This suggests that the real accuracy of stellar parameters derived from any fitting technique using theoretical models will strongly depend on the systematic errors arising from the simplifying assumptions inherent in the theoretical models. Specifically, a critical inference from our investigation is that the precise information about the wind velocity law is required to ensure reliable determination of stellar parameters. Consequently, we plan to expand the parameter space by including models with diverse values of β . This is necessary in order to enhance the accuracy of stellar wind parameter determinations.

On the technical side, we see at least two ways to achieve better accuracy in derived stellar parameters: (a) build ‘denser’ model grids; (b) improve the numerical approximation of model spectra.

In practical terms, denser model grids with smaller parameter steps can enhance the accuracy of derived stellar parameters within the 4D grid fitting framework. However, this approach demands significant computational resources and time. The latter is due to the complexity of the grid-building process, which is not easily automated.

The need for numerical approximation arises because stellar atmosphere codes cannot produce detailed spectra of all chemical elements ‘instantaneously’. While it would be ideal to avoid numerical approximations, it is currently not feasible. With this respect, the accuracy of the derived stellar parameters will improve if we manage to find a ‘better’ numerical approximation than those used in Section 2.3 of this study.

Finally, we note that when analysing observed spectra of massive stars there might be two major issues as illustrated by the numerical experiments in this study. First, the wind of a real object may have velocity profile different from that adopted in our 4D grids (β -law with $\beta = 1$). Second, its chemical composition may deviate from the abundance set used to calculate these grids. And, the ‘combined’ effect of both issues is hard to foresee. While the first issue could be handled by adding a new ‘dimension’ to the grids (no matter whether ‘globally’ or ‘lo-

cally’, as discussed above), we do not think it is feasible to adopt the same approach for handling (estimating) the chemical composition from fitting the observed spectrum of a massive star. The reason is that it is not possible to define a ‘global’ parameter which could describe the variety of changes in the spectrum due to different chemical elements. Alternatively, adding more ‘dimensions’ to the grids even only for the most abundant elements is hardly to be considered the way to go. Therefore, this ‘combined’ effect needs to be addressed in detail and the corresponding solution will likely adopt some iteration-procedure that must be carefully tested: a complex task that we plan to consider in a follow-up study.

6 Data availability

The calculated 4D grids (792 WC spectra, 432 WN spectra and 600 SMC spectra) as well as their future updates (if any) will be available from this link: https://drive.google.com/drive/u/1/folders/16gLnF2Z3abES8CPU0xI2dKBw8j58MW6_. The model spectra are in the range 1000 - 11000 Å with sampling of 1 Å.

Acknowledgements

This research is based on observations made with the International Ultraviolet Explorer (IUE), obtained from the MAST data archive at the Space Telescope Science Institute, which is operated by the Association of Universities for Research in Astronomy, Inc., under NASA contract NAS 5–26555. This research has made use of the NASA’s Astrophysics Data System, and the SIMBAD astronomical data base, operated by CDS at Strasbourg, France.

References

- Choudhury, S., Subramaniam, A., Cole, A. A., & Sohn, Y. J. 2018, *Monthly Notices of the Royal Astronomical Society*, 475, 4279
- Crowther, P. A., Rate, G., & Bestenlehner, J. M. 2023, *Monthly Notices of the Royal Astronomical Society*, 521, 585

- Fitzpatrick, E. L. 1999, *Publications of the Astronomical Society of the Pacific*, 111, 63
- Gräfener, G., Koesterke, L., & Hamann, W. R. 2002, *Astronomy & Astrophysics*, 387, 244
- Hamann, W. R. & Gräfener, G. 2004, *Astronomy & Astrophysics*, 427, 697
- Hamann, W. R., Gräfener, G., Liermann, A., et al. 2019, *Astronomy & Astrophysics*, 625, A57
- Hillier, D. J. & Lanz, T. 2001, in *Astronomical Society of the Pacific Conference Series*, Vol. 247, *Spectroscopic Challenges of Photoionized Plasmas*, ed. G. Ferland & D. W. Savin, 343
- Hillier, D. J. & Miller, D. L. 1998, *The Astrophysical Journal*, 496, 407
- Le Borgne, J. F., Bruzual, G., Pelló, R., et al. 2003, *Astronomy & Astrophysics*, 402, 433
- Niedzielski, A. & Skorzynski, W. 2002, *Acta Astronomica*, 52, 81
- Press, W. H., Teukolsky, S. A., Vetterling, W. T., & Flannery, B. P. 1992, *Numerical recipes in FORTRAN. The art of scientific computing* (Cambridge: University Press, —c1992, 2nd ed.)
- Prinja, R. K., Barlow, M. J., & Howarth, I. D. 1990, *The Astrophysical Journal*, 361, 607
- Rosslove, C. K. & Crowther, P. A. 2015, *Monthly Notices of the Royal Astronomical Society*, 447, 2322
- Sander, A., Hamann, W. R., & Todt, H. 2012, *Astronomy & Astrophysics*, 540, A144
- Sander, A. A. C., Hamann, W. R., Todt, H., et al. 2019, *Astronomy & Astrophysics*, 621, A92
- Schmutz, W., Hamann, W. R., & Wessolowski, U. 1989, *Astronomy & Astrophysics*, 210, 236
- Sundqvist, J. O., Björklund, R., Puls, J., & Najarro, F. 2019, *Astronomy & Astrophysics*, 632, A126
- van der Hucht, K. A., Cassinelli, J. P., & Williams, P. M. 1986, *Astronomy & Astrophysics*, 168, 111
- Zhekov, S. A., Petrov, B. V., Tomov, T. V., & Pessev, P. 2020, *Monthly Notices of the Royal Astronomical Society*, 494, 4525

A 4D-grid fitting of the UV-optical spectrum of WR 23

The accuracy of the derived stellar parameters of a studied object generally depends on the quality of its observed spectra. We recall that the 4D fitting procedure works with spectra in absolute flux units. Therefore, the photometric absolute uncertainties associated with the observed spectrum will have an impact on the derived stellar parameters. Additionally, the spectral resolution (and sampling) should not be very ‘crude’, because that will result in inaccurate emission line profiles which in turn would deteriorate the quality of the derived stellar wind velocity.

The distance to the studied object, along with its associated uncertainties, is another physical quantity that is important for obtaining a reliable stellar parameters. Specifically, it plays a key role in estimating stellar luminosity, which subsequently affects the derived values of both the mass-loss rate and stellar temperature. This relationship arises, because the continuum is primarily determined by the stellar luminosity. Thus, changing the distance, which leads to changes in luminosity, causes changes in the ionization structure of the stellar wind. To maintain consistency in the observed spectrum, adjustments are necessary. This involves ‘back-adjusting’ the ionization structure by modifying the mass-loss rate and stellar temperature. The latter is particularly significant as it determines the quantity of photoionizing photons emitted.

The focus of this study is not to derive stellar parameters of massive stars, however, in this appendix we provide an example how the 4D grid-fitting procedure can be applied to real observations. Therefore, in the light of the preceding discussion, WR 23 was selected. WR 23 is categorized as a Wolf-Rayet star of the WC (carbon-rich) subtype (e.g., the Galactic Wolf-Rayet Catalogue; Rosslowe & Crowther 2015⁷) at a Gaia distance of 2.3 ± 0.1 kpc (Crowther et al. 2023).

The optical spectrum of WR 23 was taken from the STELIB spectroscopic library that has an intermediate spectral resolution of $\leq 3\text{\AA}$, sampling of 1\AA , and overall absolute photometric uncertainty of 3% (Le Borgne et al. 2003).

We expanded the spectral range by making use of the

⁷Galactic Wolf Rayet Catalogue; <http://pacrowther.staff.shef.ac.uk/WRcat/index.php>

UV spectrum of WR 23 from the International Ultraviolet Explorer (IUE): the data are taken from the MAST archive (Mikulski Archive for Space Telescopes⁸). The IUE spectrum has a sampling of 1.68\AA at wavelengths $\lambda < 1979\text{\AA}$ and 2.67\AA at wavelengths $\lambda > 1979\text{\AA}$, respectively.

Our fitting procedure of observed spectra consists of the following steps.

First, we prepare the 4D grid of model spectra for the corresponding spectral binning (sampling) of the observed spectrum at hand.

Then, we derive the stellar parameters using the approach described in Section 2.3 for the nominal distance of 2.3 kpc to WR 23. Also, we derive the stellar parameters for the cases of upper (2.4 kpc) and lower (2.2 kpc) limits to the distance.

Finally, we repeat these fits for the three values of the distance as for each case we perform the 4D fitting twice to take into account the absolute photometric uncertainties: i.e., considering the flux to be by 3% higher or lower than the nominal flux.

In all the fits, we adopt the Galactic extinction curve of Fitzpatrick (1999) with $R_V = 3.1$.

The derived stellar parameters and their associated uncertainties are given in Fig. 5 and Table 4. Note that the highest contribution to uncertainties of the derived parameters is due to the errors on distance to WR 23. Because luminosity scales as the square of the distance, the highest impact is on the derived value of stellar luminosity and the uncertainties on the absolute flux then accumulate: i.e., they add extra uncertainty. But in general, the uncertainties from distance and absolute flux are somehow ‘redistributed’ between the derived values of luminosity, mass-loss rate and stellar temperature. It is worth nothing that the wind velocity remains unaffected by this redistribution, likely because the wind velocity is mostly ‘confined’ by the emission-line profiles.

Note that if any of the stellar parameters we are fitting for is already constrained from other studies, we can incorporate that prior information by keeping the parameter fixed at its known value and then proceed to fit the remaining parameters. Nevertheless, among the four fundamental stellar parameters, only the terminal wind velocity can be constrained reliably from observations.

⁸<https://archive.stsci.edu/>

Table 4: 4D grid-fitting results for WR 23.

Parameter	UV+Optical	Optical
T_* (kK)	93.86 [93.28; 97.97]	99.05 [95.58; 101.78]
$\log \dot{M}$ ($M_\odot \text{ yr}^{-1}$)	-4.559 [-4.595; -4.510]	-4.577 [-4.614; -4.545]
$\log L$ (L_\odot)	5.435 [5.360; 5.485]	5.369 [5.320; 5.433]
v_∞ (km s^{-1})	2298 [2293; 2318]	2251 [2240; 2259]
E(B-V) (mag)	0.590 [0.584; 0.593]	0.547 [0.542; 0.553]

Notes. The derived fit parameters (stellar temperature, mass-loss rate, luminosity, stellar wind velocity, reddening) with the associated uncertainties, i.e. the range of parameter value given in parentheses (see Fig. 5). Labels ‘UV+Optical’ and ‘Optical’ denote results from fitting the entire WR 23 spectrum or only its optical part.

Interestingly, the derived terminal velocity from the 4D grid-fitting, *using no a priori information about its value*, is in good correspondence with the value of 2280 km s^{-1} from the classical analysis of IUE spectra of massive stars by Prinja et al. (1990) and of 2342 km s^{-1} by Niedzielski & Skorzynski (2002). This is valid both for the fits to the entire spectrum (UV-optical) of WR 23 and only to its optical spectrum (Table 4).

In general, the results of fitting the UV-optical and only the optical spectrum of WR 23 are in acceptable correspondence between each other (see also Section 3). We attribute it to the presence of many strong emission lines, that help constrain better the physical parameters of the studied massive stars. Nevertheless, it is our understanding that the former (results from fitting the entire spectrum) should be considered more reliable.

Finally, we note that reddening curves with $R_V \neq 3.1$ can be used in our 4D-grid fits. But, this can be adopted only if corresponding information is available from other studies.

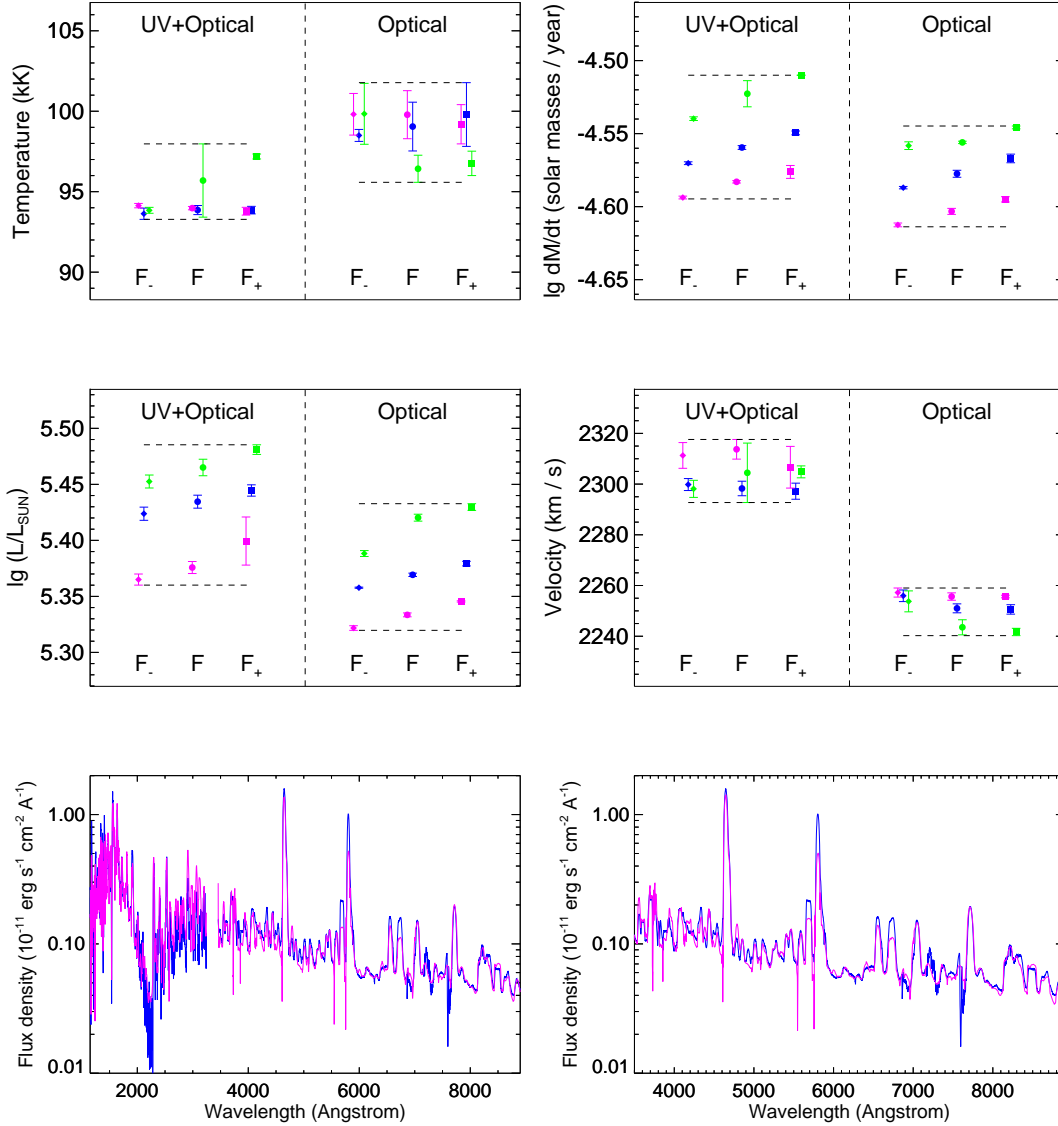


Figure 5: Derived stellar parameters for WR 23: stellar temperature (T_*), mass-loss rate ($\log \dot{M}$), luminosity ($\log L$) and terminal wind velocity (v_∞) are shown in the upper four panels. The results are color-coded as follows: values for the nominal distance to WR 23 of 2.3 kpc are shown in blue, those for the lower limit on distance (2.2 kpc) are in magenta, and those for the upper limit on distance (2.4 kpc) are in green. The results for the nominal spectra are marked by the 'F' symbol, while those corresponding to the typical absolute flux uncertainty of $\pm 3\%$ are marked by the 'F₊' and 'F₋' symbols, respectively. Error bars present the uncertainties due to the adopted numerical technique (4D grid-fitting): if not visible, the error bars are smaller than the size of the plotted symbol. The horizontal dashed lines (in black) present the accumulated errors of each parameter due to the distance and absolute flux uncertainties (see Table 4). Labels 'UV+Optical' and 'Optical' denote results from fitting the entire WR 23 spectrum or only its optical part. The lower two panels show the observed spectrum (in blue) overlaid with the best-fit model spectrum (in magenta) for the cases of nominal distance and nominal absolute flux calibration. The best-fit model spectra are calculated with *cmfgen* using the mean model parameter values as given in Table 4.

B Tests with different abundances, wind acceleration law and volume filling factor

In the figures below, we provide the results from the 4D-grid modelling (fitting) of test spectra ('perfect' observed spectra) for the objects considered in this work (WC, WN and SMC). These tests are aimed at checking the corresponding effects if chemical composition (abundances), stellar wind acceleration (β -law) and clumping (volume filling factor) in the observed objects differ from those used to build our 4D spectral grids of model spectra.

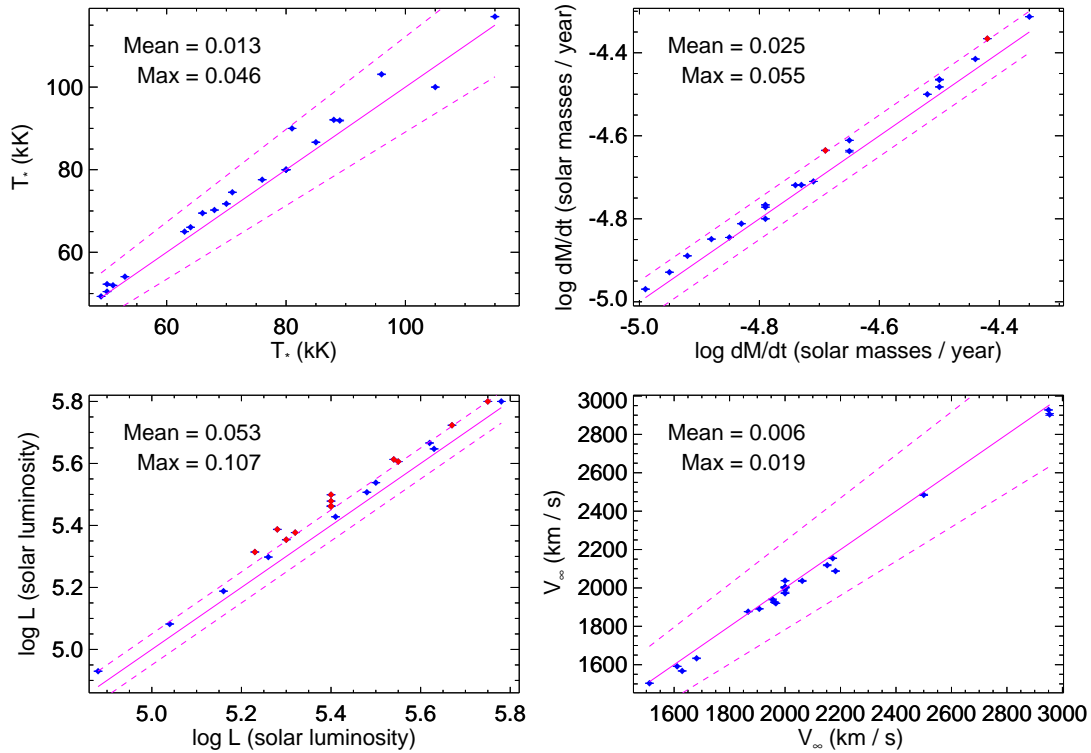


Figure 6: Test results for the ‘Add.’ set of WC abundances (‘perfect’ observed spectra): effective temperature, mass-loss rate, luminosity and terminal wind velocity. Lines in magenta colour: (a) the solid line represents the perfect correspondence between the input model parameters and their values derived from the grid-modelling; (b) the two dashed lines represent the boundary for the ± 0.05 dex absolute deviation from the expected perfect correspondence. The symbols shown in red colour are those that are beyond the boundary accuracy of 0.05 dex for the derived parameters. Mean and Max labels denote the mean absolute deviation for the test sample and its maximum value. Error bars are the standard deviation of the four minimizations adopted.

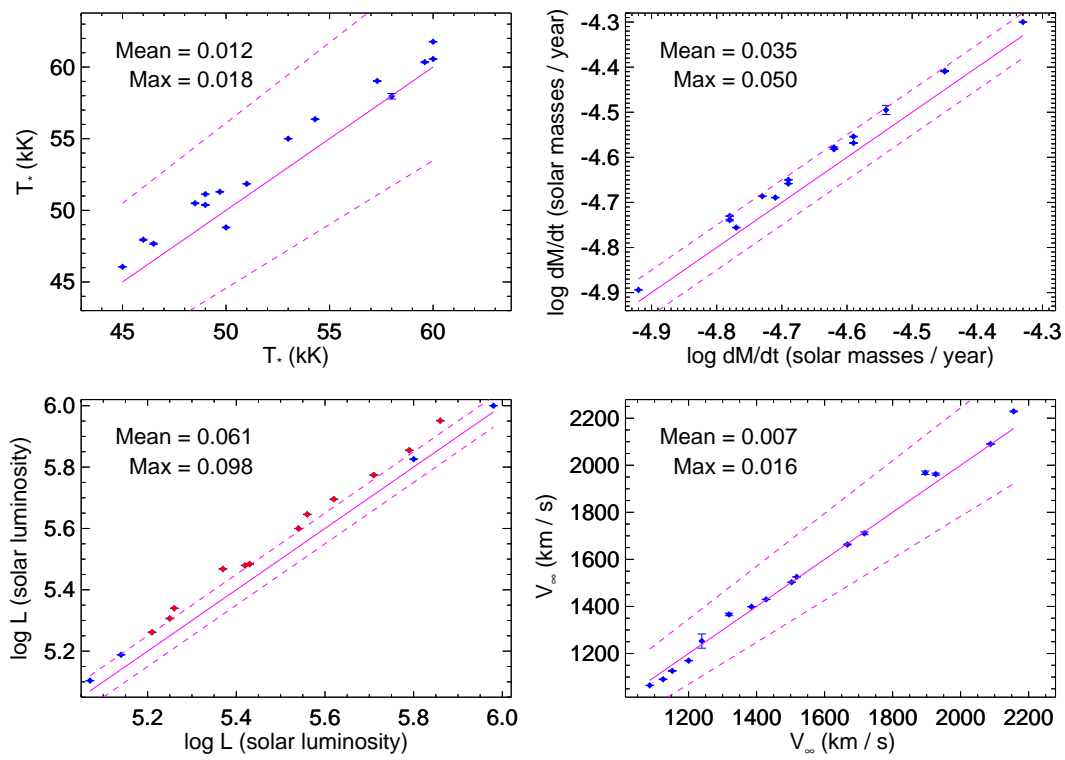


Figure 7: The same as Fig. 6 but for the ‘Add.’ set of WN abundances (‘perfect’ observed spectra).

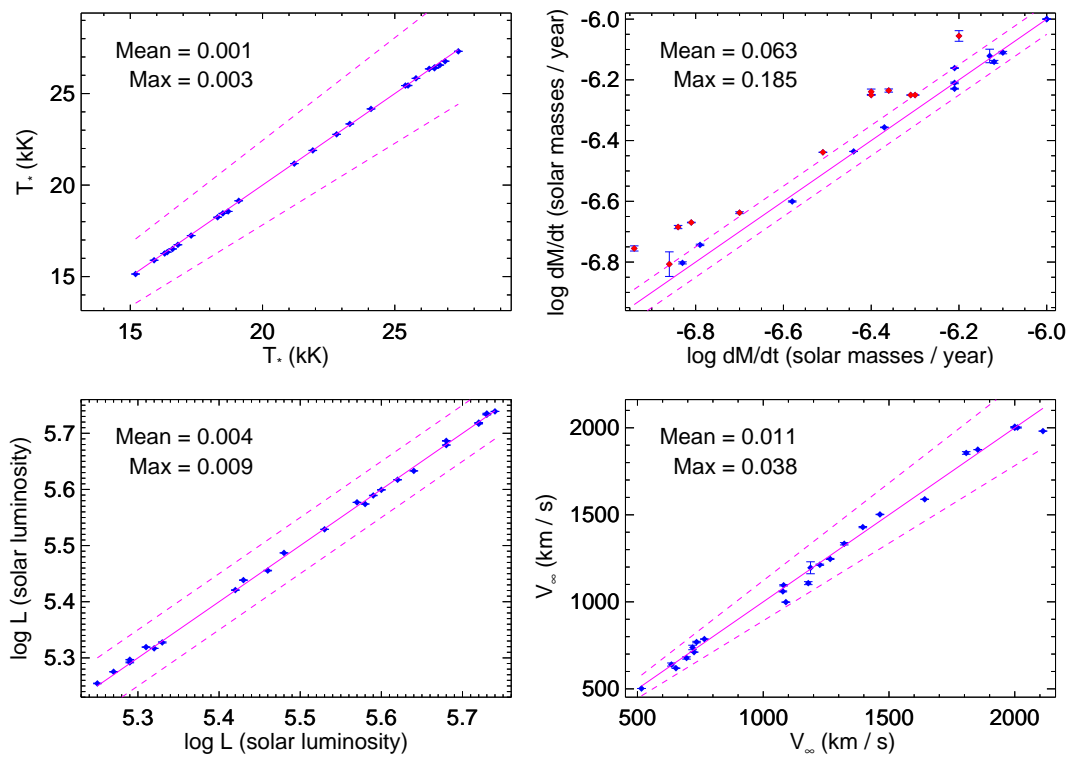


Figure 8: The same as Fig. 6 but for the 'Add.' set of SMC abundances ('perfect' observed spectra).

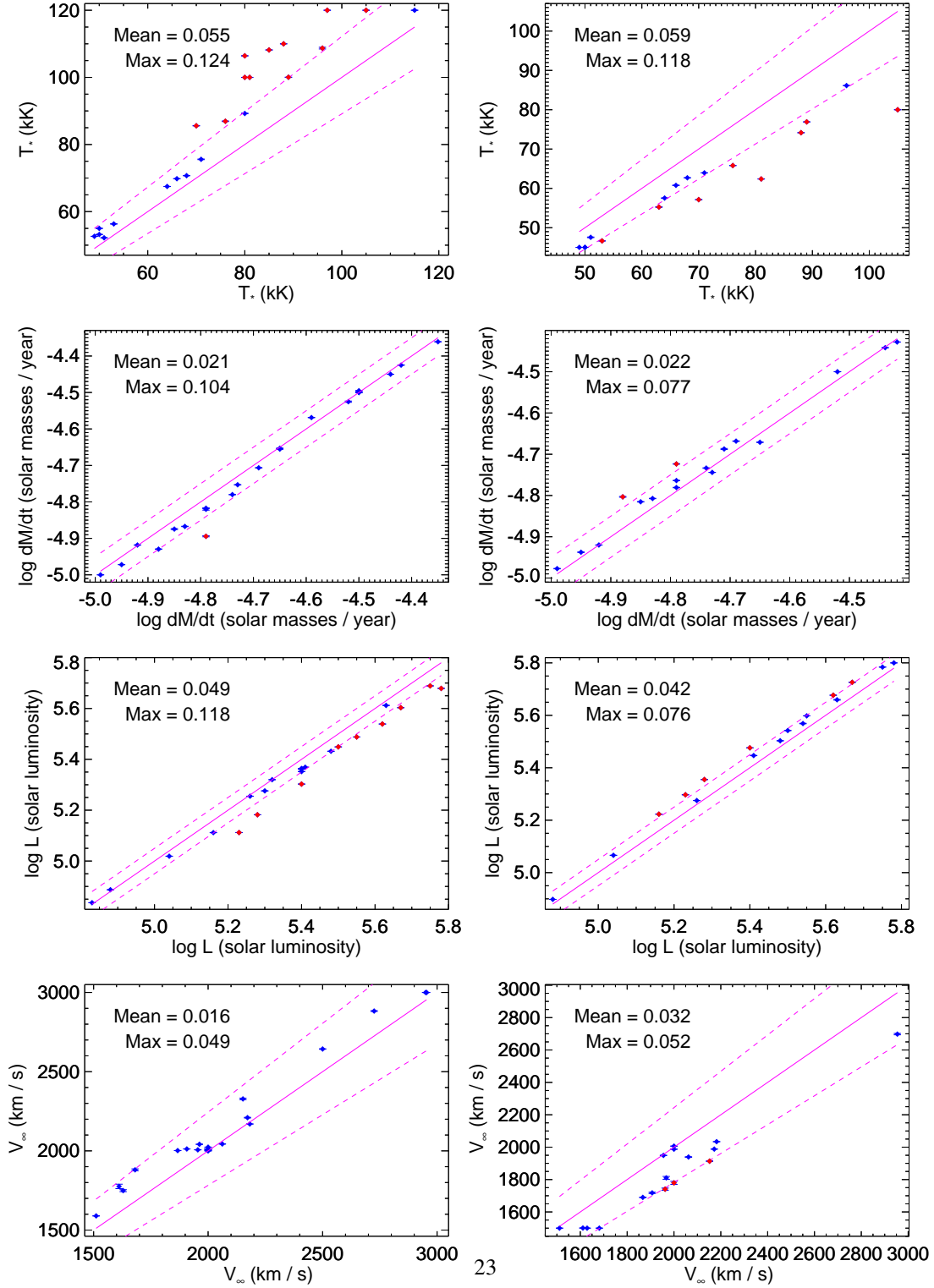


Figure 9: The same as Fig. 6 but for the WC grid and β -law with $\beta = 0.5$ (left panels) and $\beta = 2$ (right panels) ('perfect' observed spectra).

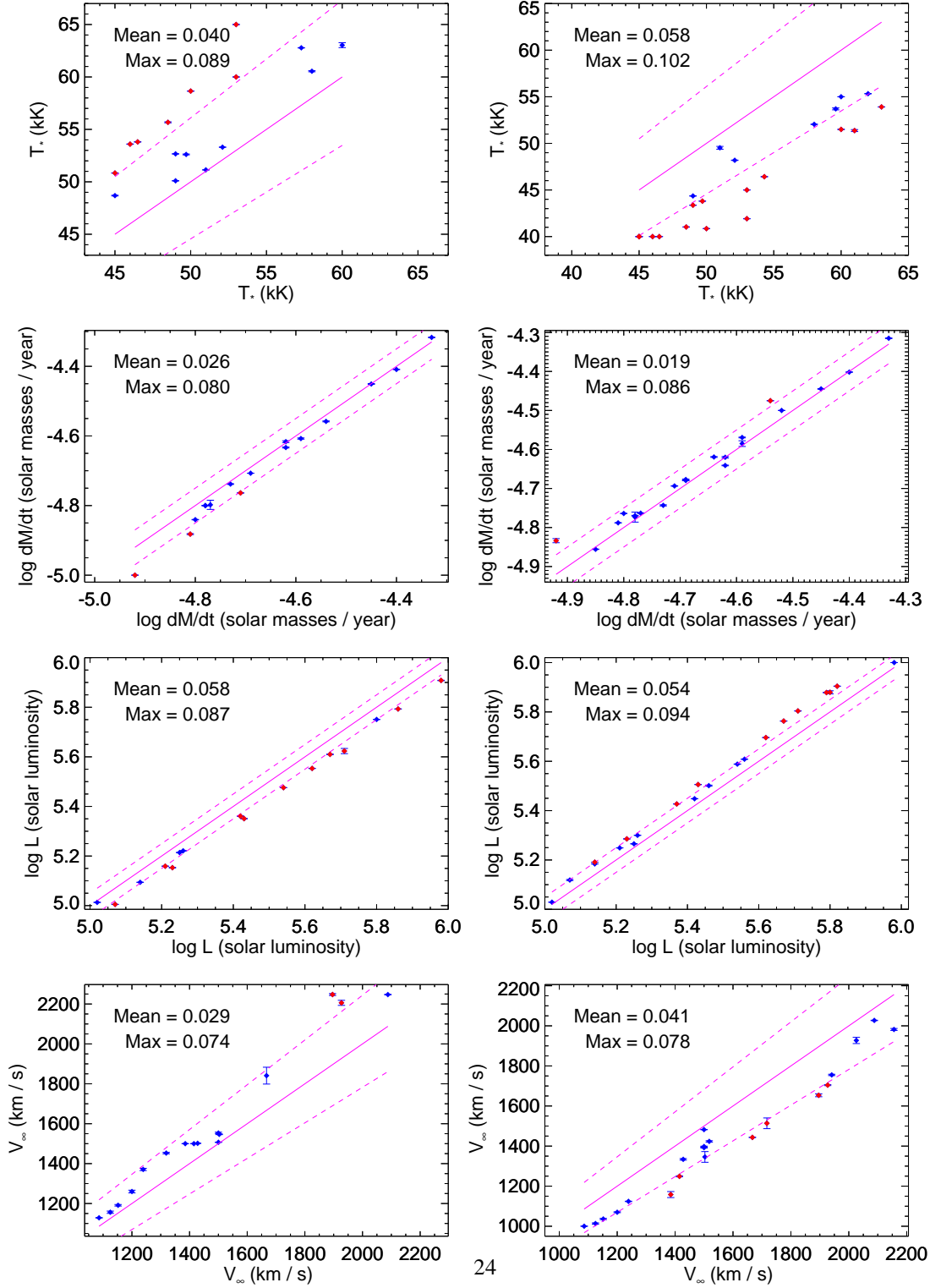


Figure 10: The same as Fig. 6 but for the WN grid and β -law with $\beta = 0.5$ (left panels) and $\beta = 2$ (right panels) ('perfect' observed spectra).

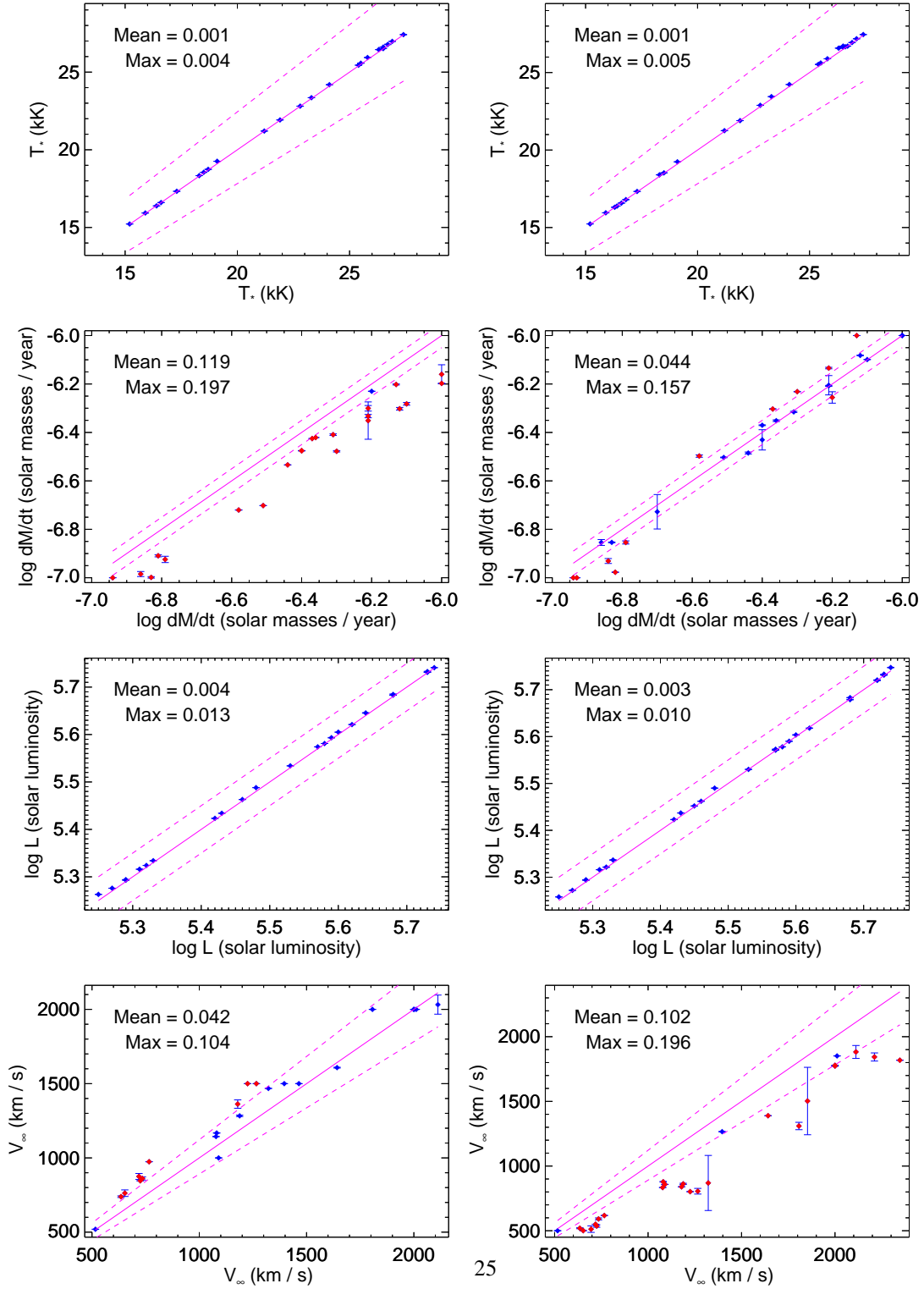


Figure 11: The same as Fig. 6 but for the SMC grid and β -law with $\beta = 0.5$ (left panels) and $\beta = 2$ (right panels) ('perfect' observed spectra).

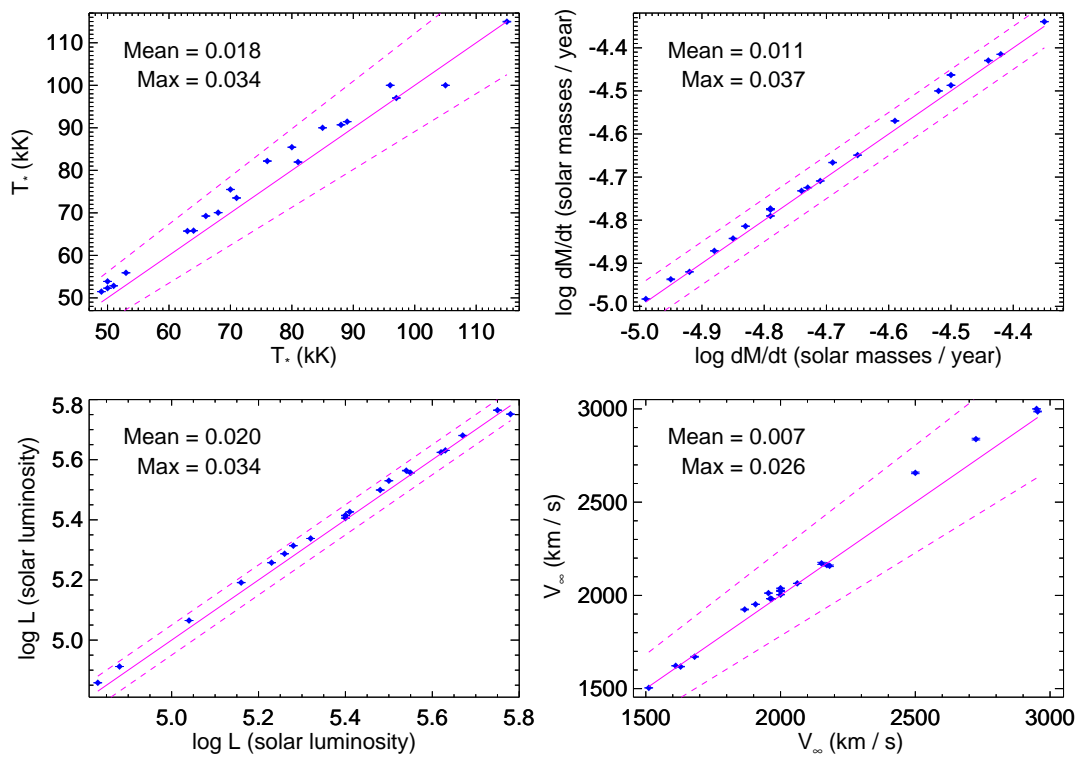


Figure 12: The same as Fig. 6 but for the WC grid and volume filling factor $f_\infty = 0.25$ ('perfect' observed spectra).

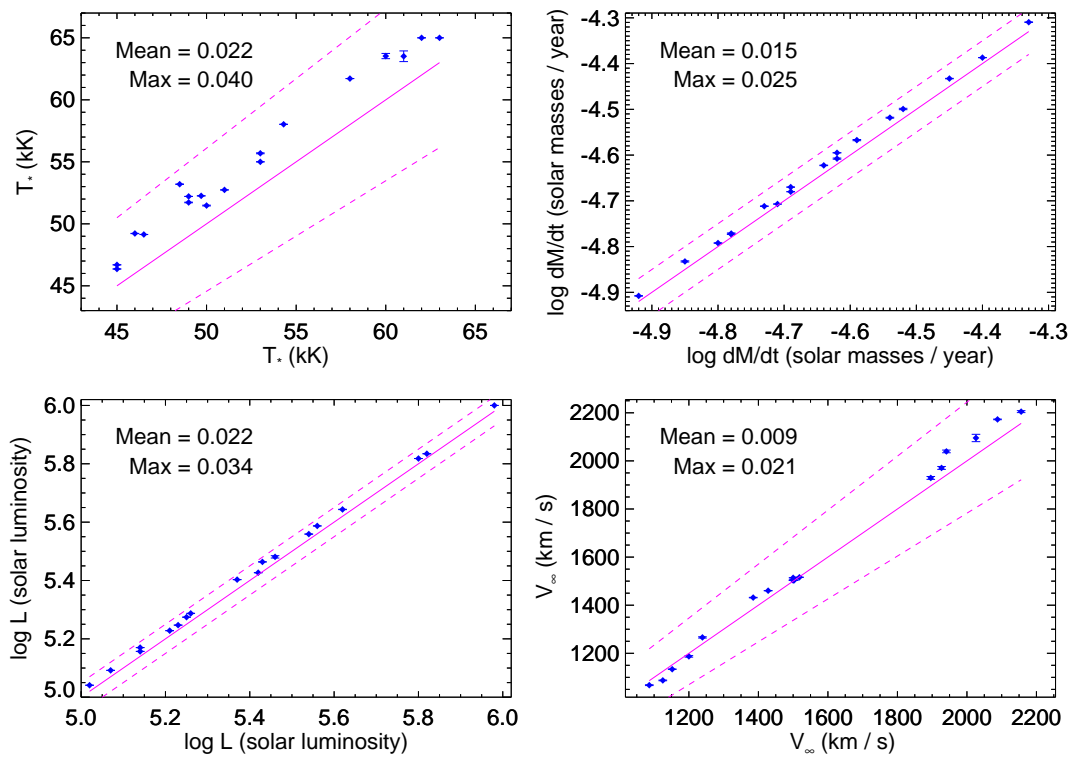


Figure 13: The same as Fig. 6 but for the WN grid and volume filling factor $f_{\infty} = 0.25$ ('perfect' observed spectra).

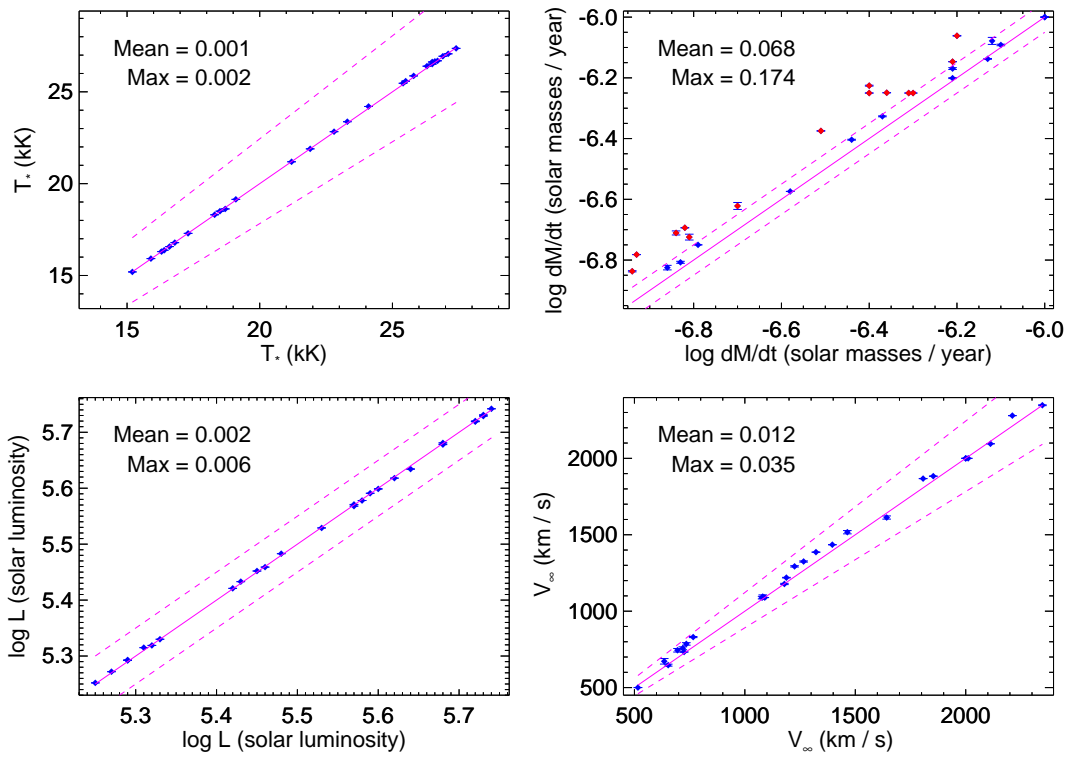


Figure 14: The same as Fig. 6 but for the SMC grid and volume filling factor $f_\infty = 0.25$ ('perfect' observed spectra).